MinEx CRC Limited
26 Dick Perry Avenue, Kensington, WA, 6151
PO Box 1130, Bentley, WA, 6102, Australia
admin@minexcrc.com.au

ABN: 66 625 533 913

MinEx CRC provides financial support to the value of $1K to promote Honours and Masters by Coursework projects that are aligned with the mission of MinEx CRC and to encourage young researchers toward a career in mineral exploration research. Projects are not restricted to MinEx CRC Participants and Affiliates.

Please note that the content of this thesis has not been subjected to peer-review and subsequent corrections.

Australian Government
Department of Industry, Science and Resources
Cooperative Research Centres Program

LONDON'S GLOBAL UNIVERSITY

CENG0037 MSc Research Project

Linking pyrite chemistry to mineralisation across the Delamerian Orogeny, South Australia

by:

Shiqi ZOU

Student's registration number: 22071474

Supervisor(s): Dr. Adrienne Brotodewo

A/Prof Caroline Tiddy

A thesis submitted to the University of London for the degree of Master of Science

Department of Chemical Engineering

University College London (UCL)

September 2023

Declaration

I, Shiqi ZOU, confirm that the work presented in this thesis is my own. Where information has been derived from other sources, I confirm that this has been indicated in the thesis.

Word count: *5800*
(excluding the title page, table of contents, references, tables, figures and appendices)

Has the written report been submitted on Moodle?

Yes

Have relevant source codes and/or raw data been submitted on Moodle?

Yes

Has the lab space used been cleaned up (if applicable)?

Yes

Shiqi ZOU	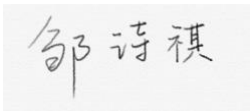	06/09/2023
.....	.....	.....
Student's Name	Student's Signature	Date

Abstract

Trace elements within pyrite is used here as geochemical indicators of mineral deposits to determine if there is potential for mineralisation in a recent drilling campaign in the Delamerian Orogen. In this paper, five pyrite samples from the recent Delamerian NDI Campaign by the Geological Survey of South Australia and MinEx CRC were collected and subjected to microscopic observation and Laser Ablation Inductively Coupled Plasma Mass Spectrometry (LA-ICP-MS) analysis. Data was compared to pyrite chemistry from known deposits around the world to determine the similarities between the samples and mineralisation potential of the region. The results of the analyses show that the pyrite is derived from both the VMS deposit and the porphyry deposit. In addition, their genesis may be associated with hydrothermal event. This research enriches the comprehension of mineralisation potential within the Delamerian Orogen, furnishing invaluable insights for targeted exploration and resource extraction within the region. Amidst the challenges of a shifting resource landscape, these findings offer a roadmap for sustainable resource discovery and utilisation.

Keywords: pyrite; geochemistry; Delamerian Orogeny; mineralising systems; VMS deposit; Porphyry deposit; mineral exploration

Contents

List of Figures and Tables

1.Introduction

The demand for critical resources is increasing as a result of the global-scale green energy transition. However, global reserves of critical resources pose a major challenge as they continue to decline[1]. The rate of discovery of economically viable deposits is rapidly declining as easily accessible surface resources are depleted[1]. As a result, the exploration frontier is shifting to deeper horizons, bringing greater costs and risks. To address some of the risks associated with deep mineral exploration, innovative technologies are being developed to assist in mineral exploration. One such technique is mineral chemistry, which involves the study of the chemical composition and properties of minerals. This approach provides valuable insights into the formation and distribution of mineral deposits and aids in identifying potential exploration targets.

Recent drilling by the Geological Survey of South Australia (GSSA) and MinEx CRC took place within South Australia on the eastern part of the Cambrian-Ordovician Delamerian Orogen[2] (Fig. 1). Traditionally, exploration efforts for base and precious metals in the Delamerian basement have been concentrated along the western margin[2]. However, preliminary data from the recent drilling campaign conducted on the eastern margin reveals promising indications of the presence of mineralisation suitable for porphyry Cu-Au and volcanic massive sulphide (VMS) deposits.

Pyrite is the most abundant sulphide phase in the Earth's crust and is commonly associated with mineralisation in a variety of deposit types found in different environments. These deposit types include VMS, orogenic Au, porphyry, shallow-forming hydrothermal, BIF and SEDEX deposits[3]. Therefore, analysing the geochemistry of pyrite can provide insight into changes in fluid composition and stratigraphic conditions. Pyrite is also an important host for a range of trace elements, including Au and Co, as well as the semimetals As, Se, Sb, Te and Bi[4]. The concentrations and ratios of Au, As and Co in pyrite have been used to infer key ore-forming processes and characterise different mineralising systems[5].

In this paper, we examine the chemical composition of five pyrite samples to provide information on the changing physiochemical conditions of fluids precipitated from pyrite and their relationship to mineralisation events. The eastern part of the Cambrian-Ordovician Delamerian Orogen in South Australia was used as a case study area, where pyrite samples were taken from a recent MinEx CRC drilling campaign. Pyrite morphology and trace and rare earth element geochemical signatures are discussed in a regional context and compared with currently published pyrite data to use pyrite to develop a new geochemical standard for exploration suitable for porphyry copper-gold and volcanic massive sulphide (VMS) deposits.

2.Geological Background

2.1 Pyrite

Pyrite is a common metallic mineral with a chemical composition of FeS_2 and often with a yellowish-brown metallic lustre on the surface[6]. It is the most common sulphide mineral in nature and is widely distributed in the earth's crust[6].

Pyrite forms under reducing conditions, this is usually in an environment with low oxygen, high sulphur content and abundant iron[7]. Pyrite usually forms through a combination of geological processes, and is commonly found in hydrothermal, sedimentary, and metamorphic environments[7]. Numerous studies have indicated that pyrite is usually associated with hydrothermal deposits[4, 8, 9]. These deposits form when hot fluids rich in dissolved minerals migrate through cracks and faults in the earth's crust. The fluids carry elements such as iron and sulphur, which can precipitate out of solution and form pyrite in the cracks and pores of rocks[7]. Pyrite can also form in sedimentary environments where organic material, such as dead plant material, is buried in the sediment[10, 11]. Under certain conditions, such as a lack of oxygen, the organic material decomposes and releases sulphur. The sulphur combines with the iron minerals present in the sediment, leading to the formation of pyrite. In metamorphic environments, existing iron-rich minerals can be subjected to heat and pressure, leading to the formation of pyrite [12].

The chemical composition of pyrite can provide valuable information on various aspects of geological processes and environmental conditions such as differences in fluid composition and formation conditions[3]. Pyrite is often found in association with valuable minerals in hydrothermal deposits, therefore can give insights into the formation of those mineralising systems[4].

The trace element compositions of pyrite can be utilised as a valuable tool in differentiating between different deposit types, such as porphyry deposits and volcanic-hosted massive sulfide (VMS) deposits during exploration[3]. VMS pyrites exhibit higher levels of elements such as Cu, Co, Pb, Se, Zn, Sn, and Bi[3], while porphyry deposit pyrites display elevated levels of Cu, Mo, Au, Ag, Re, and Te[13]. These variations can be attributed to differences in source rocks and variations in the salinity, temperature, and pH of the ore fluids[3].

2.2 Porphyry and VMS mineral deposits

Porphyry deposits are the world's most important source of Cu and Mo, as well as a major source of Au, Ag and Sn[14]. Important by-product metals include Re, W, In, Pt, Pd and Se. They account for 50-60% of world copper production and more than 95% of world molybdenum production[14]. Porphyry deposits occur as high, low to medium grade deposits. Deposits in which the primary (secondary) ore minerals are largely structurally controlled and are spatially and genetically related to feldspathic to intermediate porphyritic intrusions[15].

In porphyry deposits, mineralisation primarily occurs along fractures or within alteration zones adjacent to fractures[16]. Porphyry-type mineral deposits are formed when significant volumes of hot water, carrying trace amounts of metals, flow through permeable rocks and deposit the metals[17]. The deposition occurs as a result of the interaction between the circulating fluids and the host rocks, leading to the precipitation of minerals containing valuable metals[17].

VMS deposits are another important type of mineral deposit with distinctive characteristics. They are significant sources of base metals such as copper, zinc, lead, and also provide valuable quantities of precious metals like gold and silver[18]. Most of the world's VMS deposits are small, with about 80% of known deposits in the 0.1-10 megatonne range[19].

VMS deposits are formed from hydrothermal fluids generated by volcanic activity. These fluids are rich in sulphur and metals, and they are usually ejected from undersea volcanic vents[18]. When the hot fluids encounter cold seawater, they cool rapidly, causing the metals and sulphur to precipitate and form mineral deposits[18]. The mineralogy of VMS deposits is complex, with many different minerals present. These deposits typically consist of layers of metallic sulphides, such as chalcopyrite, sphalerite and galena, mixed with vein minerals such as pyrite, quartz and feldspar[19].

2.3 Overview of the Delamerian Orogeny

The Delamerian Orogeny (c.514-490Ma)[20] is an exceptional geotectonic event that occurred in Australia and affected a fractured plate margin encased in Neoproterozoic and Early Cambrian sediments. This tectonic event led to the inversion of Cambrian rocks within a subduction zone environment [20].

The Delamerian Orogen is widely distributed in southern Australia, particularly in the eastern part of South Australia, and the western part of New South Wales, Victoria and Tasmania (Fig.1)[21]. The Delamerian Orogen is most evident in South Australia, where it is widely exposed and buried underneath thick cover sequences [22]. The

Adelaide Fold Belt is the main outcrop of this geological orogenic belt, including the Adelaide Hills, Fleurieu Peninsula and Kangaroo Island. The formation of this terrain was caused by the Cenozoic uplift[23], exposing only the first part of the orogenic process[22].

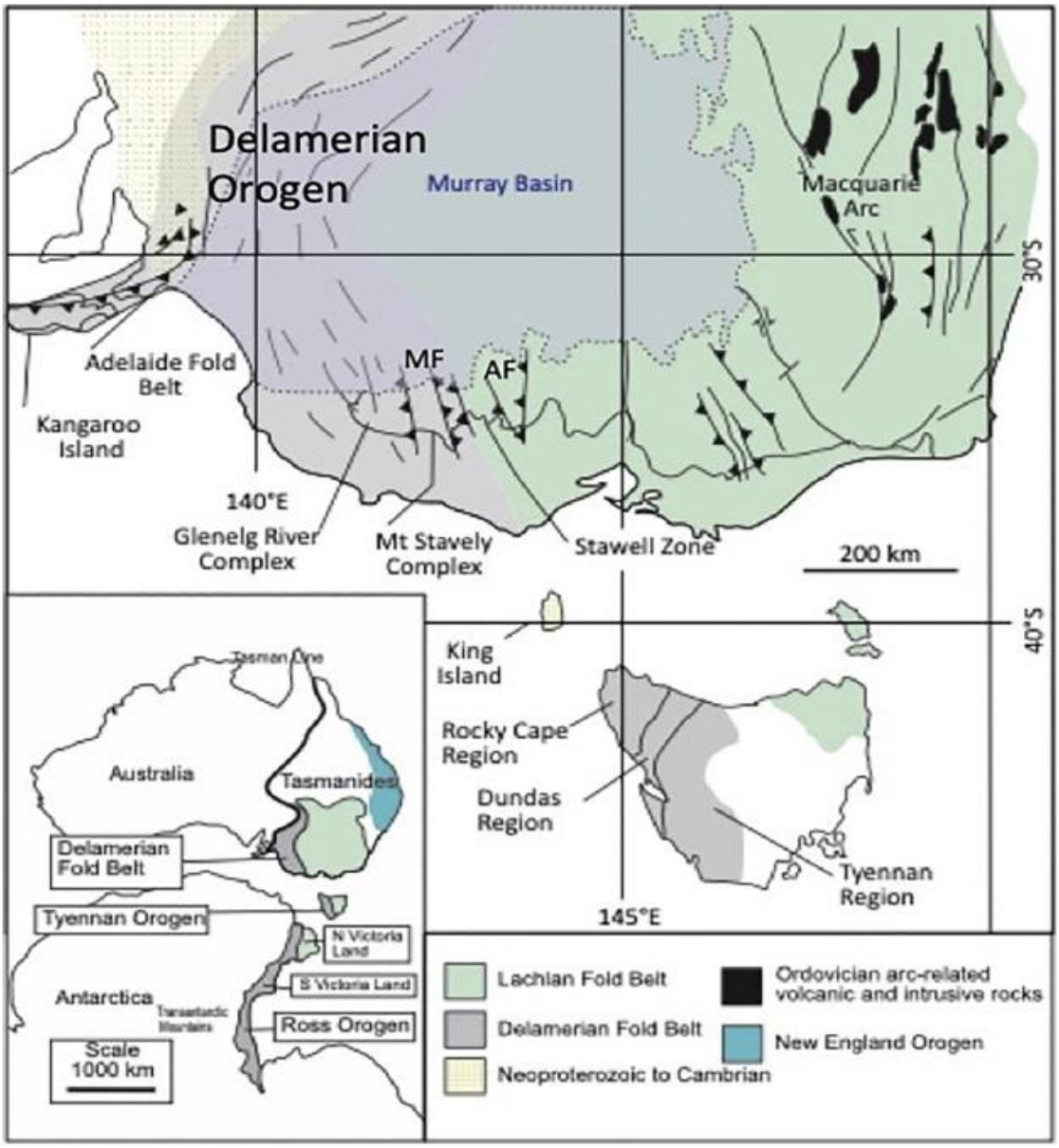

Fig. 1 Regional map of Delamerian Orogen[21]

The Delamerian Orogen hosts high-quality gold, copper, lead and zinc deposits in igneous and less metamorphosed sedimentary rocks[24]. Samples for the study came from the Alawoona and Quondong Vale drilling areas of the Murray Basin(Fig.2)[25].

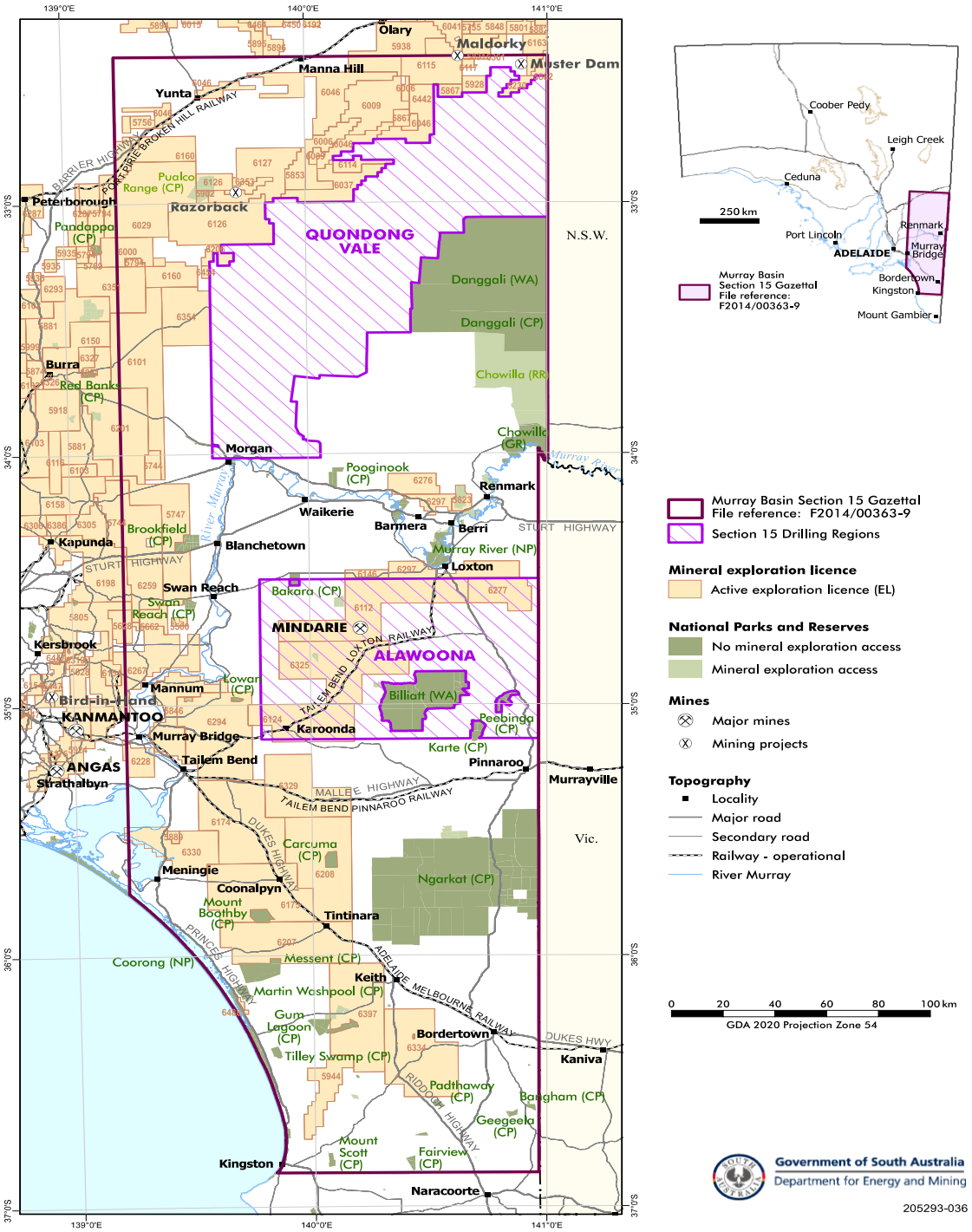

Fig. 2 Delamerian National Drilling Initiative (NDI) drilling regions[25]

The Murray Basin region has a limited number of drillholes that intersect the underlying basement, and the density of these drillholes significantly decreases towards the eastern border with South Australia [2]. The available drillhole data indicates that the basement primarily consists of mafic to intermediate volcanic and volcaniclastic rocks with varying degrees of deformation. Additionally, there are fewer occurrences of felsic volcanic rocks, as well as felsic and mafic intrusives that are believed to have formed during the Delamerian Orogeny[2]. Metasedimentary and metavolcanic rocks, correlated with the Moralana Supergroup, are also present in the basement[2].

Studies involving the geochemistry and geochronology of these igneous rocks have revealed that the mafic to intermediate volcanics predominantly exhibit characteristics associated with back-arc environments. However, some igneous rocks display geochemical signatures indicating a subduction-related origin, suggesting either a primary subduction origin or derivation from a lithosphere that has been modified by subduction processes[2]. These findings suggest that the Delamerian basement in the Murray Basin of South Australia likely represents a transition zone from a back-arc setting to a continental volcanic arc setting. Consequently, the region has the potential to host various deposit styles, including volcanic-hosted massive sulfide, epithermal, Carlin-style and orogenic gold, Cu-Au-Mo porphyry, base metal sedimentary exhalative, and Ni-Cu-platinum group element magmatic sulfides[2].

3. Methodology

The study employed a comprehensive methodology to analyse pyrite samples from the base of the Renmark Group in the Murray Basin (Quondong Vale and Alawoona). Five samples collected from the Delamerian NDI Campaign by the Geological Survey of South Australia were examined. The study began by making mounts of the sample cores. Second, microscopic observations using high-resolution imaging techniques provided insight into the distribution and characteristics of pyrite. Third, scanning electron microscopy (SEM) provided insight into surface features and crystal structure. Fourthly, laser ablation inductively coupled plasma mass spectrometry (LA-ICP-MS) was used for the chemical analyses of trace and rare earth elements. Finally, the analyses were supplemented by comparing the experimental data with data from previous studies.

3.1 Sample selection and preparation

A total of 5 samples from the basement, underneath the Murray Basin were used in this study. The Geological Survey of South Australia provided sample collection and drill core from their recent Delamerian NDI Campaign with MinEx CRC. Samples were collected as slices of core, approximately 10 cm in length. The intervals were selected had pyrite various pyrite generations present. Samples were labelled: 4331854 from Quondong Vale and 4331855, 4331857, 4331858, 4331859 from Alawoona.

All samples were mounted as chips or individual grains in resin and prepared as polished discs suitable for microscopic observation. Discs were polished and coated with carbon for further analysis.

3.2 Microscope

Microscopic observation of pyrite samples plays a vital role in understanding their distribution and characteristics. The method captures high-resolution images of pyrite samples from different angles and magnifications. At the same time, proper illumination and focus settings are ensured to obtain the best image quality.

3.3 SEM

Scanning electron microscopy (SEM) is a powerful technique for studying the morphology and microstructure of materials at high resolution[26]. In the case of pyrite, SEM can provide valuable insights into its surface characteristics and crystal structure. The internal structure of pyrite was imaged by backscattered electron (BSE) imaging on a Hitachi benchtop SEM at the Microscopy Laboratory, University of South

Australia to identify the crystallisation history of individual grains by internal textural features and to further analyse specific growth stages.

3.4 LA-ICP-MS

Laser Ablation Inductively Coupled Plasma Mass Spectrometry (LA-ICP-MS) was used to collecte pyrite trace and rare earth element chemistry. The instrumentation used was Agilent 7900x with attached RESOlution LR 193nm Excimer laser system at the University of Adelaide. The reference materials employed during the analysis included STDGL3[27], which was utilised for the assessment of chalcophile and siderophile elements within sulfide samples. Additionally, GSD-1G[28] was used for the analysis of elements across silicates, carbonates, and oxides. Reference materials were analysed in blocks of every 20 unknown analyses. The analysis of these materials was conducted using a round beam with a diameter of 51 µm and a frequency of 10 Hz. This approach was chosen to minimise the impact of downhole fractionation. The laser fluence applied for the analysis of STDGL3 averaged 2.7 J/cm^3, while for GSD-1G, the average laser fluence was 3.5 J/cm^3. Samples were ablated for 90s, with 30s of that being the background.

The complete list of analysed elements and their associated isotopes remains consistent across all sessions, regardless of the method employed. The elements and isotopes analysed are as follows: ^{23}Na, ^{24}Mg, ^{27}Al, ^{29}Si, ^{31}P, ^{34}S, ^{39}K, ^{43}Ca, ^{45}Sc, ^{49}Ti, ^{51}V, ^{53}Cr, ^{55}Mn, ^{57}Fe, ^{59}Co, ^{60}Ni, ^{65}Cu, ^{66}Zn, ^{71}Ga, ^{75}As, ^{77}Se, ^{85}Rb, ^{88}Sr, ^{89}Y, ^{90}Zr, ^{93}Nb, ^{95}Mo, ^{107}Ag, ^{109}Ag, ^{111}Cd, ^{118}Sn, ^{121}Sb, ^{125}Te, ^{137}Ba, ^{140}Ce, ^{157}Gd, ^{178}Hf, ^{181}Ta, ^{182}W, ^{185}Re, ^{195}Pt, ^{197}Au, ^{202}Hg, ^{205}Tl, ^{206}Pb, ^{207}Pb, ^{208}Pb, ^{209}Bi, ^{232}Th, and ^{238}U. All data was processed using the software Iolite, and data was reported in ppm.

3.5 Collection of data from literature

In this study, the results of other analysed samples of pyrite were also collected through literature[29]. These data are largely derived from Gregory *et al*. (2019) who used laser ablation-inductively coupled plasma-mass spectrometry to differentiate between deposit types and barren sedimentary pyrite[29]. The majority of these data originate from two large projects for pyrite analysis funded by the Geological Survey of Western Australia and the Geological Survey of South Australia[29]. The LA-ICP-MS information originated from various sources. These sources encompass published peer-reviewed papers, project reports, along with newly discovered data from the Chalkidiki porphyry Cu district in Greece and the Lady Loretta SEDEX deposit in Australia[29].

4. Results

4.1 Sample descriptions

Sample 4331854 (Fig.3 A) is from drillhole NDI_QVD20 from 252.23 to 252.3 metres. A mount is used in this sample. This is a sample with pyrite in breccia where there are some volcanics. Pyrite is recognised within the brecciate framework as dipping crystals. A breccia is a fractured rock matrix indicative of a dynamic depositional environment in which rock fragments are forcefully broken and subsequently cemented together. Most of these pyrite grains are cubic, but some are rounded. The pyrite is fine-grained but interconnected with distinct cracks in the centre(Fig.3 C). The average size of pyrite grains is about 40 microns(Fig.3 B).

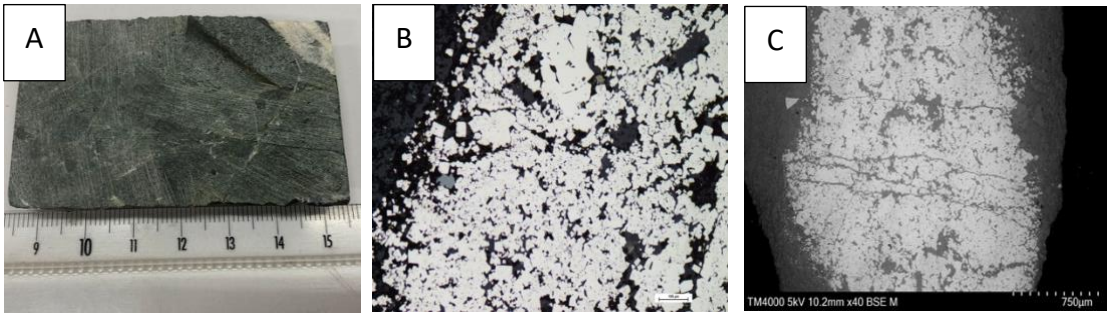

Fig. 3 Sample 4331854. A) Drill core sample displaying pyrite in brecciated volcanics; B) Photo micrograph display disseminated pyrite grains; C) SEM image of pyrite

Sample 4331855 (Fig.4 A) is from drillhole NDI_AWD02 from 270 to 270.1 metres. Two mounts are used in this sample (4331855M1 and 4331855M2). This sample is a pyrite-bearing sediment. The sediments themselves represent the layered accumulation of detritus and organic material over time, facilitated by sedimentary processes such as lithification and compaction. Pyrite is clearly visible in the samples and has a distinctive light golden to brassy yellow metallic lustre. The pyrite in 4331855M1 has large grains up to 32 mm (Fig.4 C). The grains are cracked (Fig.4 B). Microscopic examination of the samples also revealed the presence of pyrite crystals that exhibit different morphologies (Fig.4 D,E and F). The pyrite in 4331855M2 has different sizes of grains up to 750 microns (Fig.4 F).

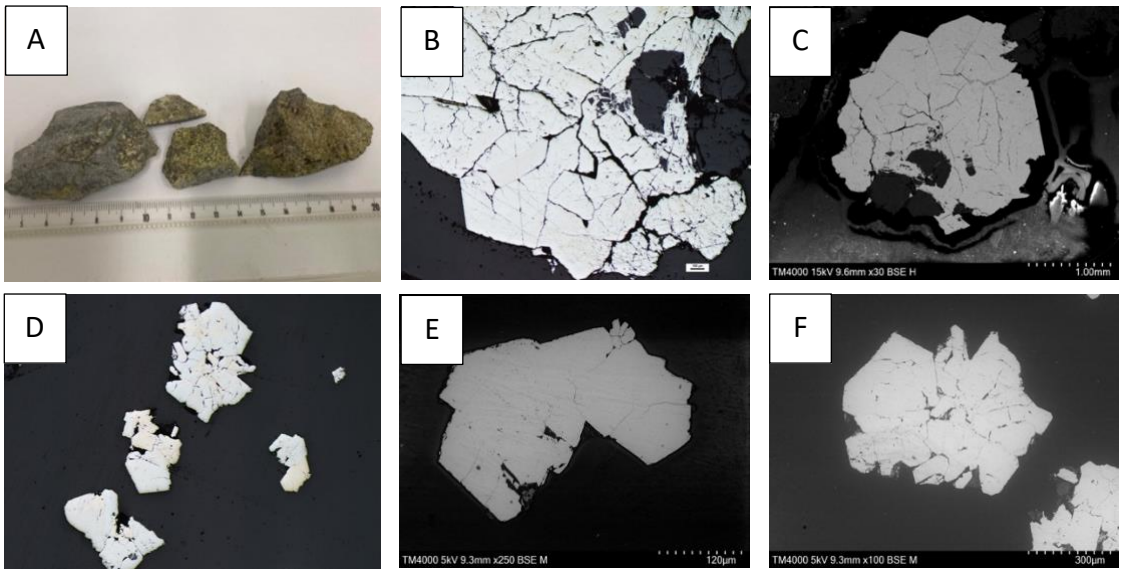

Fig. 4 Sample 4331855 A) Drill core sample displaying pyrite in the sediments; B) Photo micrograph display 4331855M1 pyrite grains; C) SEM image of 4331855M1 pyrite; D) Photo micrograph display 4331855M2 cubic pyrite grains; E&F) SEM image of 4331855M2 pyrite

Sample 4331857 (Fig.5 A) is from Hole NDI_AWD05 from 364.33 to 364.39 metres. Two mounts are used in this sample (4331857M1 and 4331857M2). The sample examined consists of pyrite embedded in detrital fragments within a brecciated matrix. Pyrite was observed in discrete detritus fragments of various sizes and lithologies. The matrix that surrounds these pyrite-bearing debris is characterised by a brecciated structure, indicating fragmentation and angular assemblages of rock fragments. The matrix material may consist of a combination of rock debris fragments, mineral particles, and potentially altered compositions that form a cohesive bonding material used to embed and stabilise the detrital fragments within the overall rock structure. The pyrite grains in 4331857M1 are more fractured, while the pyrite grain in 4331857M2 is a large cubic grain up to 34 mm.

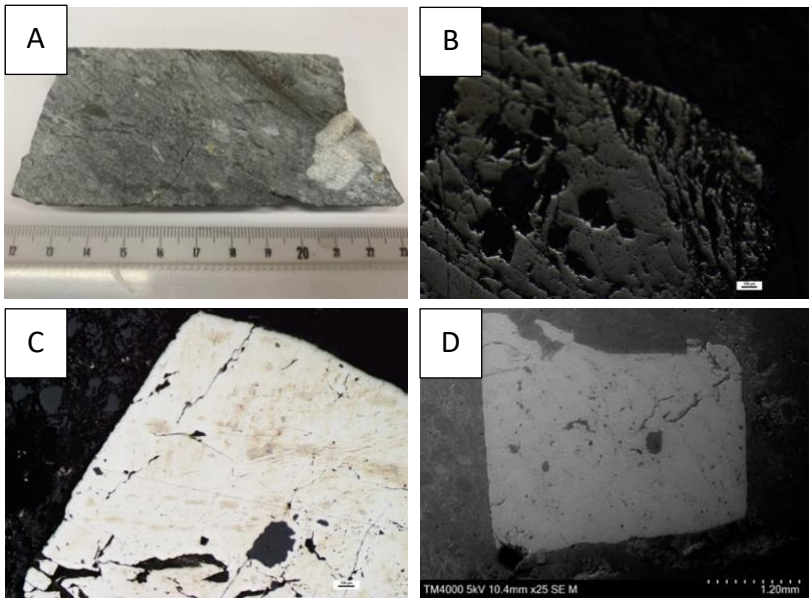

Fig. 5 Sample 4331857 A) Drill core sample displaying pyrite embedded in detrital fragments within a brecciated matrix; B) Photo micrograph display 4331857M1 disseminated pyrite grains; C) Photo micrograph display 4331857M2 cubic pyrite grain; D) SEM image of 4331857M2 pyrite

Sample 4331858 (Fig.6 A) is from Hole NDI_AWD06 from 271.15 to 271.22 metres. Samples examined include primary pyrite occurrences within the volcaniclastic matrix. Two mounts are used in this sample (4331858M1 and 4331858M2). The pyrite in 4331858M1 and 4331855M2 both have different sizes of cubic grains. These pyrite grains have some tiny cracks and irregular holes on them (Fig.6 C and E). In addition to silver-white pyrite grains in sample 4331858M1, there are chalcopyrite grains encased in rounded grains (Fig.6 B and D). The pyrite in sample 4331858M1 has large grains up to 1750 microns (Fig.6 C), while the pyrite in sample 4331858M2 has large grains up to 2.1 mm (Fig.6 F). In addition, some pyrite occurrences are located in close proximity to veins.

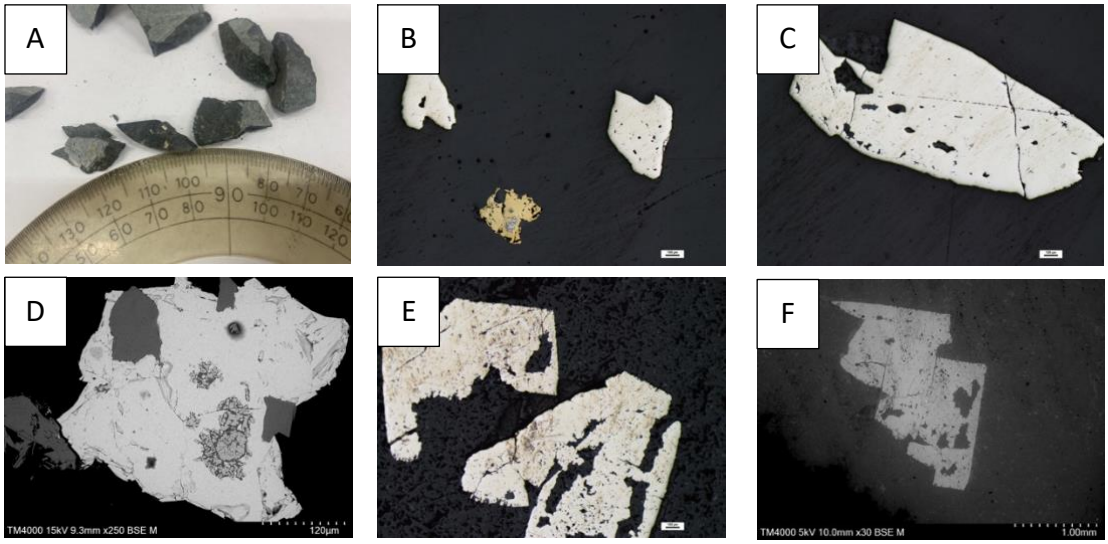

Fig. 6 Sample 4331858 A) Drill core sample displaying pyrite within volcaniclastic matrix; B&C)Photo micrograph display 4331858M1 pyrite grains; D) SEM image of 4331858M1 pyrite; E) Photo micrograph display 4331858M2 pyrite grains; F) SEM image of 4331858M2 pyrite

Sample 4331859 (Fig.7 A) is also from Hole NDI_AWD06, but from 252.74 to 252.81 metres. The sample is pyrite associated with quartz veins. It is quartz cemented medium-coarse-grained pyrite. Two mounts are used in this sample (4331859M1 and 4331859M2). The material in the sample that possesses milky-white translucency and prominent crystal formations is quartz veins, which are conduits for mineral-laden aqueous solutions through the lithic matrix (Fig.7 A). Sample 4331859M1 has large square pyrite grains surrounded by chalcopyrite (Fig.7 B). The grains are distinctly textured and have cracks and small holes. The pyrite located at the edges is ringed (Fig.7 C). Sample 4331859M2 contains both disseminated pyrite grains (Fig.7 D and F) and large cubic pyrite grains (Fig.7 E). The pyrite in sample 4331859M2 has large grains up to 400 microns (Fig.7 E).

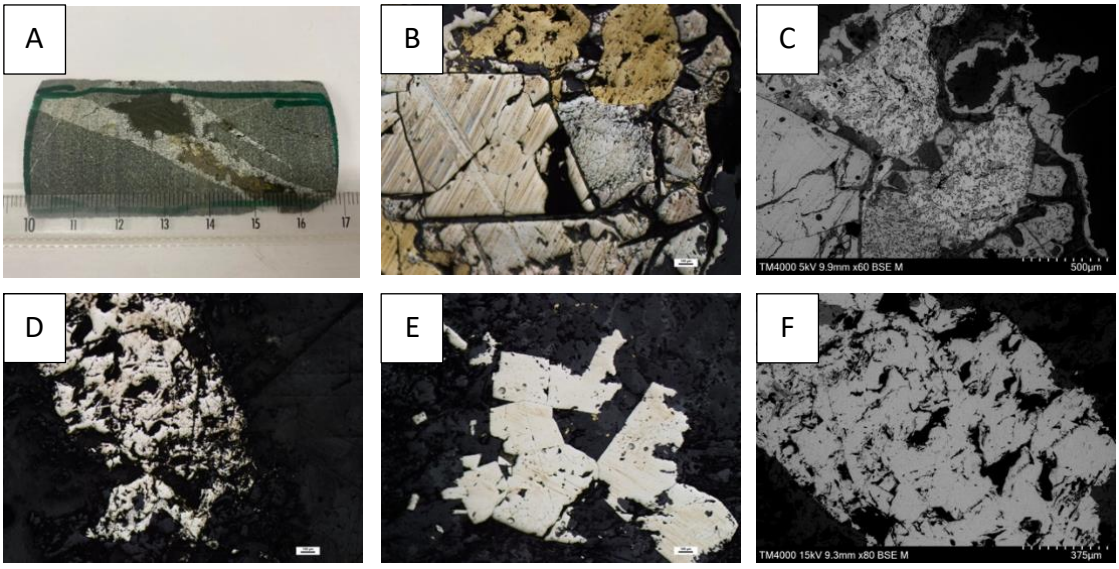

Fig. 7 Sample 4331859 A) Drill core sample displaying pyrite associated with quartz veins; B) Photo micrograph display 4331859M1 pyrite grains; C) SEM image of 4331859M1 pyrite; D&E) Photo micrograph display 4331859M2 pyrite grains; F) SEM image of 4331859M2 pyrite

4.2 LA-ICP-MS

4.2.1 Results of trace element analyses of 5 pyrite samples

The results of trace element analyses of pyrite from the five samples are shown in Table 1. Overall, the trace element analyses show that the different types of pyrite have different Co, Ni, Cu, Zn, As, Mo, Ag, Sb, Te, Au, Tl, and Pb contents (Fig. 8).

Pyrite mount from sample 4331854 has high mean values of Co, Ni, As, Mo, Ag, Sb, Te, Au, Tl, Pb and medium Cu, Zn compared to other samples (Table 1).

Sample 4331855 contains two different pyrite mounts. M1 and M2 have consistently high mean values of Co, Ni, Cu, Zn and low Mo, Au, Tl compared to other samples (Table 1). There are some differences in the chemical composition of the two mounts, with M1 having higher Cu than M2, and lower Ni, Zn, Au, Tl, Pb contents than M2.

Sample 4331857 contains one pyrite mount, which has high mean values of Au, Tl, Pb and low Co, Ni, Cu, Zn, As compared to other samples (Table 1).

Sample 4331858 contains two different pyrite mounts. M1 and M2 have consistently high mean values of Co, and low Ni, Zn, Te compared to other samples (Table 1). There are some differences in the chemical composition between them, with M1 having higher Co, Cu, than M2, and lower Mo, Sb, Te, Au, Tl, Pb contents than M2.

Sample 4331859 contains two different pyrite mounts. M1 and M2 have consistently high mean values of Cu, Zn and low Ni compared to other samples (Table 1). There is some variation in chemistry between the two mounts, where M1 has higher Cu, Zn, Mo, Te and lower Co, Ni, Au, Tl, Pb than M2.

Sample	Statistic	Co (ppm)	Ni (ppm)	Cu (ppm)	Zn (ppm)	As (ppm)	Mo (ppm)	Ag (ppm)	Sb (ppm)	Te (ppm)	Au (ppm)	Tl (ppm)	Pb (ppm)
4331854	n	21	21	21	21	21	21	21	21	21	21	21	21
	Max	340	69	2810	5.4	5.56	32.7	1.13	0.108	86.1	1215	1119	1174
	Min	28.9	0.626	20.3	0.01	0.277	1.34	0.072	0.0015	0.056	70	68	68
	Mean	169.961905	17.3431429	663.77619	0.58866667	3.21619048	17.0190476	0.59280952	0.0489	20.1179048	548.961905	518.238095	530.52381
	Median	160	14.4	526	0.199	3.94	19.1	0.6	0.053	16.9	584	547	560
4331855_M1	n	17	17	17	17	17	17	17	17	17	17	17	17
	Max	1030	25	5430	0.049	0.45	3.5	1.52	0.009	0.85	14.8	11.7	11.3
	Min	0.014	0.74	295	0.005	0.0033	0.014	0.043	0.0011	0.0025	0.0032	0.00315	0.00225
	Mean	77.3686471	3.99705882	1216.88235	0.01026471	0.05055588	0.47908824	0.35264706	0.0019	0.08261471	2.60145	2.38799706	2.32366176
	Median	0.68	1.11	956	0.009	0.0095	0.093	0.244	0.0015	0.0051	1.07	1.12	1.14
4331855_M2	n	38	38	38	38	38	38	38	38	38	38	38	38
	Max	3130	111	808	26.5	2.26	3.31	3.31	0.091	0.261	177	178	174
	Min	0.033	0.58	0.23	0.0044	0.0016	0.011	0.011	0.0015	0.0023	0.048	0.034	0.0315
	Mean	85.030027	10.6056757	73.9336486	2.59847703	0.08857297	0.43433784	0.24148649	0.00406216	0.02757297	7.95462162	7.02867838	7.53038108
	Median	0.202	6.26	2.84	0.33	0.0155	0.133	0.077	0.0015	0.0078	0.751	0.44	0.65
4331857_M2	n	26	26	26	26	26	26	26	26	26	26	26	26
	Max	7.9	12.9	570	0.016	0.102	1.86	0.86	0.042	0.092	28.4	27.4	27.4
	Min	0.068	0.82	50.6	0.00465	0.00205	0.0175	0.112	0.0013	0.0023	0.0064	0.0048	0.0068
	Mean	2.03430769	3.08269231	129.884615	0.00741538	0.03300385	0.73926923	0.355	0.00975385	0.0191	11.79665	11.1188	11.4735231
	Median	1.805	2.375	80.2	0.00675	0.02215	0.729	0.3265	0.00645	0.0123	10.11	9.49	9.79
4331858_M1	n	22	22	22	22	22	22	22	22	22	22	22	22
	Max	900	35	1180	0.009	0.45	1.4	1.3	0.0087	0.0294	22.2	21.1	21.1
	Min	0.025	0.57	144	0.0044	0.002	0.0155	0.086	0.0015	0.00265	0.0019	0.0028	0.0024
	Mean	102.119682	4.08909091	448.968182	0.00613636	0.06200227	0.17213636	0.54668182	0.00267273	0.00609773	3.45760909	3.23607727	3.322225
	Median	0.51	1.17	377	0.00525	0.0066	0.048	0.485	0.0015	0.003975	1.045	0.77	1.015
4331858_M2	n	20	20	20	20	20	20	20	20	20	20	20	20
	Max	8.2	6.8	958	0.0155	0.203	8.3	0.72	0.042	0.92	38	36	36
	Min	0.035	0.82	50.6	0.0049	0.00205	0.0175	0.112	0.0015	0.00295	0.0064	0.0048	0.0068
	Mean	2.29494737	2.19157895	252.436842	0.00753947	0.04609737	1.09397368	0.34536842	0.00824211	0.06756053	10.3561526	9.81104211	10.0630789
	Median	1.76	1.25	149.2	0.007	0.0154	0.6	0.34	0.0043	0.0102	9.4	8.9	9.1
4331859_M1	n	30	30	30	30	30	30	30	30	30	30	30	30
	Max	11.6	34.3	5610	34.11	1.62	60.8	7.9	0.0145	51.7	18.4	17.3	17.8
	Min	0.012	0.78	0.45	0.00495	0.0016	0.012	0.082	0.0015	0.0021	0.00185	0.00205	0.0019
	Mean	1.10364286	2.72535714	1476.76071	3.58393036	0.07910536	14.4380893	0.71410714	0.00197143	12.0535893	1.69019821	1.39156071	1.57683214
	Median	0.098	1.185	312.4	0.0115	0.01105	0.3425	0.206	0.0015	0.01695	0.267	0.2665	0.267
4331859_M2	n	41	41	41	41	41	41	41	41	41	41	41	41
	Max	1030	25	6480	1.019	0.45	59	2.23	0.0112	4.75	252	239	248
	Min	0.014	0.572	0.25	0.00485	0.0015	0.014	0.033	0.0011	0.0022	0.0032	0.00315	0.00225
	Mean	41.637425	4.38405	951.934375	0.04106625	0.03742	2.3926625	0.3768	0.0021975	0.22843375	9.99899125	9.23397375	9.63830625
	Median	0.65	1.315	693.5	0.009	0.0095	0.1825	0.252	0.0015	0.00905	2.19	1.408	1.972

Table 1 Results of trace element analyses of 5 pyrite samples

4.2.2 Trace element discrimination diagrams

Pyrite trace elements ratios have been recreated after Gregory et al. (2019), which used pyrite chemistry to discriminate between Iron Oxide Copper-Gold (IOCG), Sedimentary Ejecta Deposit (SEDEX), Volcanogenic Massive Sulphide (VMS), orogenic gold, and porphyry deposits.

Figure 8A displays Cu vs Zn bivariate plot. Pyrite chemistry from most samples overlaps except sample 4331854 which has a higher Cu and Zn content. The other samples were low in Zn and Cu, but sample 4331855 had a relatively slightly higher Zn content.

Figure 8B shows a bivariate plot of As vs Mo, with samples 4331855 and 4331857 having significantly lower levels of As than the other samples. Samples 4331857, 4331858, and 4331859 have very low levels of Mo, below the detection limit.

Figure 8C shows a bivariate plot of Ag vs Pb, where there is a positive relationship between the two elements. Sample 4331854 has higher Ag vs Pb content than the other samples. All other samples have overlapping chemical compositions. All other samples have relatively low levels of Ag and Pb, with sample 4331859 being extremely low.

Figure 8D shows a bivariate plot of Au vs Te where sample 4331854 has significantly higher Au content than the other samples. Sample 4331855 has significantly lower Te glowing than the others. The other samples overlap and have Au content below the detection limit.

Figure 8E shows a Ni vs Co bivariate plot with a positive relationship. Sample 4331855 has lower levels of Ni vs Co than the other samples, and more Ni than Co. Both chemistries overlap for the other samples. All other samples have overlapping chemical compositions with relatively high levels of Co and Ni.

Figure 8F shows a bivariate plot of Sb vs Tl, where sample 4331854 has significantly more Sb vs Tl than the other samples along with sample 4331859. The other samples have overlapping and relatively low levels of both chemistries.

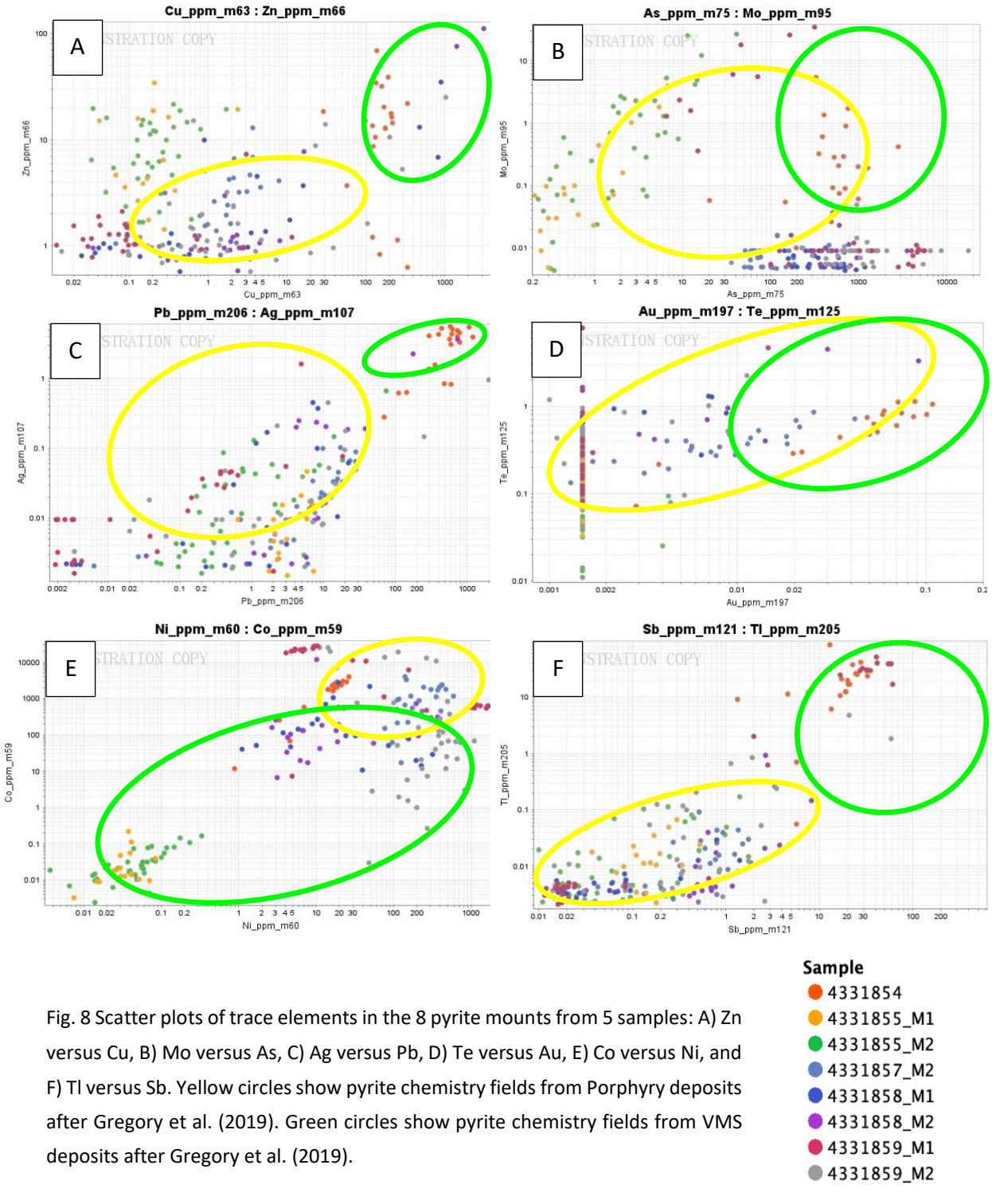

Fig. 8 Scatter plots of trace elements in the 8 pyrite mounts from 5 samples: A) Zn versus Cu, B) Mo versus As, C) Ag versus Pb, D) Te versus Au, E) Co versus Ni, and F) Tl versus Sb. Yellow circles show pyrite chemistry fields from Porphyry deposits after Gregory et al. (2019). Green circles show pyrite chemistry fields from VMS deposits after Gregory et al. (2019).

5. Discussion

The diverse forms of pyrite structure and the way trace elements are dispersed within it effectively mirror the makeup and physical-chemical characteristics (such as temperature, salinity, pH, fS_2, fO_2, etc.) of the mineral-forming fluids during various phases. As a result, pyrite holds potential as an indicator mineral for deciphering the nature of these mineral-forming fluids[30].

5.1 Pyrite textures associated with mineralisation

The pyrite in sample 4331854 has a small grain size, which suggests that it formed under conditions where the mineral crystals had limited space to grow. Fine-grained textures can indicate rapid crystallisation or the presence of other minerals that restrict pyrite crystal growth[31]. The interconnected nature of the pyrite grains suggests that the pyrite formed in a manner that allowed for mineral growth to be interconnected. The grains are mostly cubic with distinct cracks in the centre (Fig.3 C). This suggests that some form of stress or deformation has affected the sample after pyrite formation[32]. These cracks could have formed due to changes in temperature, pressure, or other geological processes. They may also indicate that the pyrite crystals experienced internal strain during their growth[32].

Sample 4331855 is the presence of pyrite in the sedimentary matrix. The presence of large pyrite grains, some up to 32 mm in size, suggests that these pyrite crystals may have formed under specific conditions that allowed for the growth of larger crystals. This could indicate a slower crystallisation process or the availability of ample space for crystal growth[31]. The cracks in these grains (Fig.4 B) might be indicative of post-crystallisation deformation or stress within the rock[32]. The observation of different pyrite crystal morphologies suggests that pyrite in this sedimentary rock may have crystallised under varying chemical and physical conditions[33]. Different crystal forms can be indicative of different growth environments, temperatures, and pressures. The presence of multiple morphologies could suggest changing conditions during the formation of the pyrite[33].

Sample 4331857 is pyrite in a breccia matrix. The presence of pyrite in detrital fragments suggests that the pyrite grains were introduced into the rock after the detrital fragments had already formed[34]. This could be due to processes like mineral deposition or replacement in a pre-existing rock[34]. The brecciated structure of the matrix suggests that the rock has undergone fragmentation and the angular assemblages of rock fragments have been cemented together[35]. This can occur in various geological settings, including impact events, fault zones, or other tectonic processes[35]. The results description notes that the pyrite grains in 4331857M1 are more fractured, while the pyrite grain in 4331857M2 is a large cubic grain up to 34

mm. This contrast in pyrite grain characteristics may indicate variations in the conditions of pyrite formation. The fractured pyrite in 4331857M1 might suggest some deformation or alteration after pyrite crystallisation, while the large cubic grain in 4331857M2 might represent a distinct stage of pyrite growth[31].

Sample 4331858 examined includes primary pyrite occurrences within the volcaniclastic matrix, demonstrating either a primary genetic origin or symbiosis with contact metamorphosed volcanic rocks. The presence of pyrite grains with different sizes suggests that pyrite in this sample may have formed under changing environmental conditions. The presence of tiny cracks and irregular holes on the pyrite grains (Fig.6 C and E) may indicate that the pyrite has experienced post-crystallisation alterations or deformation[32]. The presence of chalcopyrite grains within the rounded grains (Fig. 6 B and D) suggests that it may be possible to show that chalcopyrite and pyrite formed at different times, and that the rounded grains may be mineral aggregates that formed under specific conditions[36]. The presence of pyrite in the vicinity of the veins suggests a possible association with hydrothermal activity[37]. Veins are usually formed by the deposition of minerals that have migrated through rock fractures by hydrothermal fluids into the rock formation[37]. In this case, the formation of pyrite may be the result of these hydrothermal processes.

Sample 4331859 is from the same hole as sample 4331858, which is somewhat shallower than sample 4331858. The relationship between pyrite and quartz veins in the sample is a common phenomenon in geology. The associated quartz veins could be associated with hydrothermal activity in the region, therefore pyrite that is host within this vein may also be associated with that mineralising hydrothermal event[37]. Furthermore, pyrite is associated with other sulphides such as chalcopyrite and contain are more porous texture, which may be indicative of crystallisation from a hydrothermal fluid[36].

5.2 Pyrite chemistry associated with mineralisation

Pyrite is often found in association with valuable minerals in hydrothermal deposits, therefore the chemistry of pyrite can give insights into the formation of those mineralising systems[4]. A study by Gregory et al. (2019) collated pyrite chemistry from around the world from different deposits to discriminate between deposit types and highlight key compositional differences between them (Fig. 9).

Pyrite samples from the Delamerian NDI have been plotted to reproduce the plots after Gregory et al. (2019) to determine if the samples from this case study area have pyrite characteristics of these mineralising systems, in particular, VMS and Porphyry mineral deposits (Fig. 8 and 9). The analysis of various bivariate plots (Cu vs Zn, As vs Mo, Ag vs Pb, Au vs Te, Ni vs Co, and Sb vs Tl) in Figure 9 reveals distinct chemical

patterns within the samples. Sample 4331854 stands out with higher levels of Cu, Zn, Ag, Pb, Au, and Sb compared to the rest, suggesting potential mineralogical variations. On the other hand, sample 4331855 exhibits lower levels of As, Te, Ni, and Co, indicating a unique composition. Furthermore, samples 4331857, 4331858, and 4331859 consistently display lower concentrations of Mo, while sample 4331859 also exhibits elevated Sb and Tl levels. These findings point to the heterogeneity of the samples' chemical compositions, indicating potential differences in geological origins or processes. The overlap in chemistries among most samples underscores some underlying similarities, highlighting the need for further investigation to uncover the factors driving these variations.

In broad terms, pyrite found in medium- to low-temperature hydrothermal deposit types (VMS and SEDEX) typically exhibits elevated levels of most trace elements compared to pyrite sourced from higher-temperature hydrothermal deposit types (such as porphyry Cu, IOCG, and orogenic Au). This pattern is visualised in Figure 9, which depicts scatter plots showcasing relationships like Zn-Cu, Mo-As, Ag-Pb, and Tl-Sb[29]. Conversely, pyrites associated with porphyry Cu, IOCG, and orogenic Au generally manifest lower concentrations of Zn, Cu, Mo, Ag, Pb, Tl, and Sb[38].

The SEDEX and VMS deposits can be distinguished from other types of deposits by comparing Cu and Zn data[29]. This is because the Cu and Zn contents of these two deposits are one to two orders of magnitude higher (Fig.9 A). Thus, sample 4331854 has significantly higher Cu and Zn contents than the other samples (Fig.8 A), and could be from either the SEDEX or VMS deposits. In addition, Zn is higher in SEDEX while Cu is higher in the VMS deposit. Sample 4331854 has higher Cu (Fig.8 A). Therefore, it is inferred that they are from the VMS deposit.

The significantly lower As values can be used to distinguish the IOCG and porphyry copper deposits from other minerals (Fig.9 B). Therefore, sample 4331855 and sample 4331857 may be from IOCG or porphyry copper deposits (Fig.8 B). Co and Ni in sulphide minerals have long been used to determine the origin of pyrite[39], with porphyry copper pyrite being enriched in Ni and the IOCG being enriched in Co. Sample 4331855 is enriched in Ni along with sample 4331857 (Fig.8 E), and is therefore inferred to be from a porphyry copper deposit.

In addition, by mapping the area of elemental data distribution for the samples in Figure 8 to the area of elemental data distribution for the porphyry deposits (yellow circles) and VMS (green circles) in Figure 9, i.e., by overlaying the yellow and green circles in Figure 9 onto Figure 8, it can be seen that the area of sample 4331854 is fitted to the data for the porphyry deposits (yellow circles), and the area of sample 4331855, sample 4331857, sample 4331858, and sample 4331859 are fitted to the data for the VMS deposits (green circles).

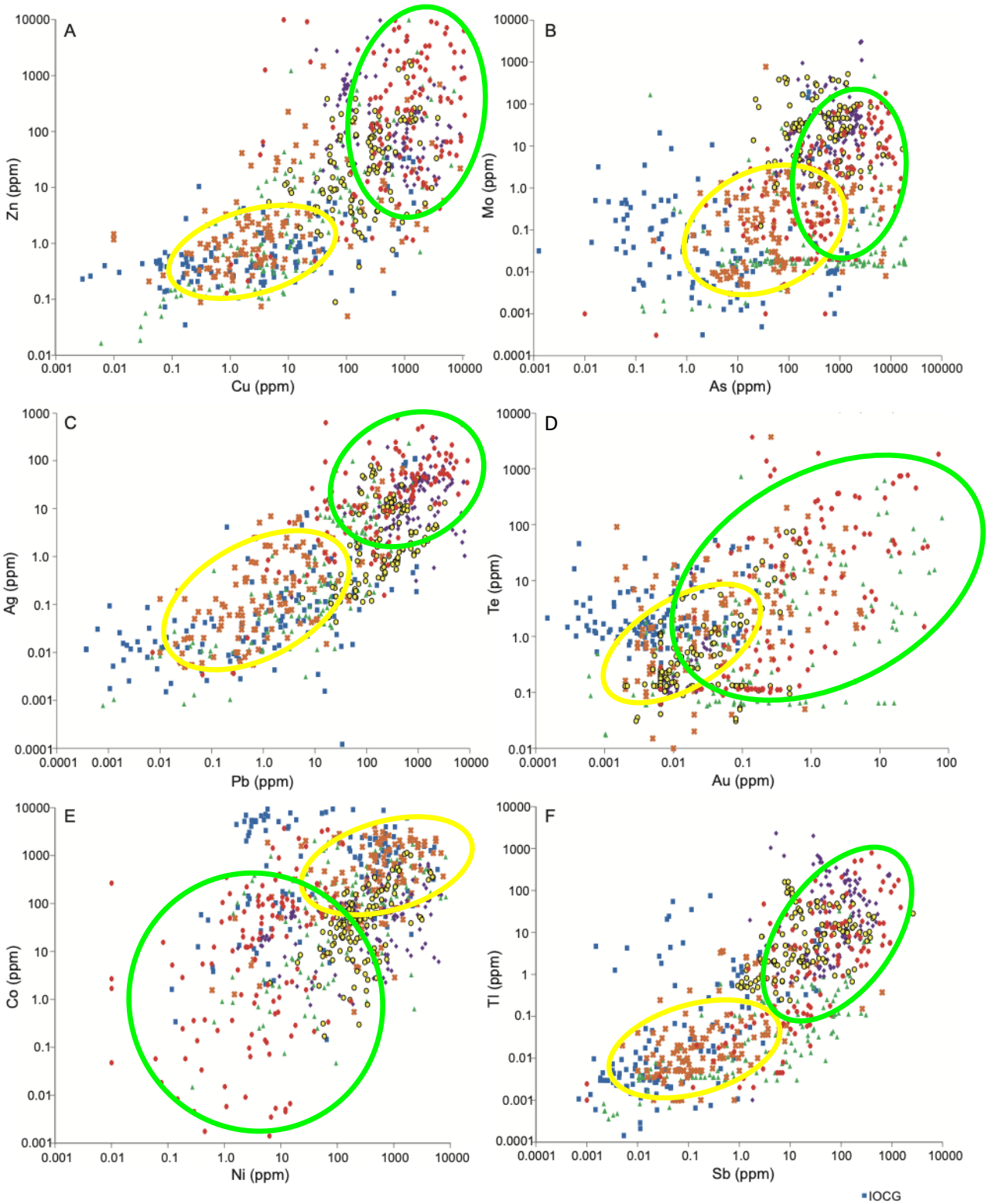

Fig. 9 Scatter plots of trace elements in pyrite used in training data set for the ore deposit type Random Forests classifier: A) Zn versus Cu, B) Mo versus As, C) Ag versus Pb, D) Te versus Au, E) Co versus Ni, and F) Tl versus Sb. Plots after Gregory et al. (2019)

In summary, sample 4331854 show similarity to VMS deposit mineralising systems and sample 4331855, sample 4331857, sample 4331858, sample 4331859 are similar to porphyry mineralising systems.

5.3 Mineralisation potential in the Delamerian and future work

The Delamerian region in Australia shows promise for hosting both VMS and porphyry style mineralisation. Notable porphyry prospects in this region include Netley Hill and Anabama Hill in South Australia[40]. Additionally, there are recognised VMS prospects like Grasmere in New South Wales and Mount Ararat in Victoria[41]. Examination of pyrite specimens obtained from the Delamerian National Drilling Initiative within a relatively uncharted section of the Delamerian orogen unveils promising indications of potential VMS and Porphyry mineralisation systems. This assertion is supported both by the pyrite samples retrieved from the Alawoona and Quondong Vale regions, which highlight VMS potential, and by the sample collections amassed during the campaign, further underscoring the presence of these mineralising systems[36, 37]. Based on the geochemical comparison of pyrite in this study, samples from the Alawoona area (sample 4331855, 4331857, 4331858 and 4331859) show potential for porphyry style of mineralisation. Additionally, sample 4331854 from the Quondong drilling area shows potential for VMS style of mineralisation through pyrite chemistry. Further analytical work on these pyrite samples provides an avenue to reveal the mineralised potential of this unexplored area. Various steps can be taken to deepen understanding and depict the extent of the mineralisation potential.

Firstly, an extended drilling campaign could be undertaken, which could provide an opportunity to validate the results obtained from the initial drilling campaign. This is important to confirm the presence, distribution and characterisation of the mineralisation indicated by the initial drilling. Obtaining more data points through additional drilling will reduce uncertainty and provide greater confidence in the accuracy of the results. This may include systematic drilling of areas of interest, core sampling and detailed geological and geochemical analyses.

More comprehensive analysis of pyrite samples can yield valuable insights into mineralisation processes. This may involve examination of isotopic compositions, trace element associations and mineral inclusion studies. These analyses can provide information on the conditions under which mineralisation occurred and its relationship to the surrounding rock layers. For example, differences in the composition of time-resolved laser ablation profiles can be attributed to varying mechanisms through which metals are incorporated into pyrite. Trace elements can be classified into three distinct groups based on their respective binding mechanisms in VMS pyrite[42]. These groups encompass the following: Micro- or nanoscale inclusions, consisting of Cu, Zn, Pb, Ba, Bi, Ag, and Sb. Non-stoichiometric substitution

involving As, Tl, Au, and Mo. Elements characterised by stoichiometric substitution for S (Se and Te) and Fe (Co and Ni).

While pyrite is an excellent indicator of mineralisation, other minerals associated with the deposit can also provide important information. Analysis of a range of minerals, including chalcopyrite, sphalerite and galena, can provide a more complete understanding of the mineralisation process and potential ore composition[43]. Each mineral reflects a different aspect of the mineralisation process. Different minerals can form at different stages of mineralisation due to variations in fluid composition and conditions. By studying a range of minerals, researchers can reconstruct the fluid evolution and sequence of mineral deposition. This helps to decipher the geological events that influenced the formation of the sediments.

Comparison of the chemical and mineralogical characteristics of the samples with samples from identified mines in the Delamerian can provide valuable background information. Similarities in the type of mineralisation can potentially be identified by comparing mineral compositions, alteration patterns and trace element assemblages between the samples and samples from known mining areas. This can provide clues about the geological setting, tectonic processes and fluid sources that may have led to mineralisation in the study area. If comparative analyses show strong similarities to known mineralised areas, this may indicate that similar mineralisation processes are at work. This information can guide targeted exploration efforts and help identify potential areas of interest for further investigation and potential resource extraction.

In summary, the Delamerian Orogen's mineralisation potential is evidenced by pyrite samples and known prospects. Further exploration through extended drilling, thorough analysis of pyrite and associated minerals, and comparative studies can unravel the geological history and unlock the full mineralisation potential of this region.

6. Conclusions

The study employed a comprehensive methodology to analyse pyrite samples from the Delamerian NDI Campaign by the Geological Survey of South Australia, to determine the fertility of this under-explored case study area. Pyrite textures and chemistry from these NDI samples are associated with mineralising events and considerable enrichment in key elements which are similar to reported pyrite compositions from known Porphyry and VMS deposits around the world.

This suggests this part of the underexplored Delamerian Orogen shows promise for hosting both VMS and porphyry mineralisation. VMS prospects like Grasmere and porphyry prospects like Netley Hill and Anabama Hill support this potential. However, further exploration and analysis are needed to confirm these findings. Extended drilling campaigns detailed geochemical studies, and mineralogical analyses of various minerals associated with the deposits are recommended. Comparing findings with established mining areas can provide valuable context and insights into the geological processes that led to mineralisation. In essence, comprehensive exploration and analysis will shed light on the mineralisation potential of the Delamerian Orogen, guiding future resource extraction efforts.

7. Acknowledgements

First and foremost, I would like to express my heartfelt gratitude to my dissertation supervisors, Dr. Adrienne Brotodewo and Associate Professor Caroline Tiddy, for their unwavering guidance, invaluable insights, and continuous support throughout my research journey.

This research was conducted as part of the MinEx CRC project, and I am grateful for the opportunity to be a part of this collaborative effort to advance the field of mineral exploration.

I extend my sincere appreciation to Microscopes Australia for providing the necessary instrumentation for my research. Special thanks to technician Alex Anthony Cavallaro for their expertise and assistance in operating the equipment.

I also would like to acknowledge the contributions of Sarah Gilbert from Adelaide Microscopes Inc., whose support and expertise significantly enhanced the quality of my research.

I am deeply grateful to the professors at University College London and the University of South Australia for their guidance and collaboration during my postgraduate studies.

Finally, I want to extend my warmest thanks to my family and my boyfriend Yin He for their support, encouragement, and understanding throughout my studies.

Your collective contributions have been instrumental in the successful completion of this research, and for that, I am truly thankful.

8. References

[1] National Research Council, *Mineral Resources and Sustainability: Challenges for Earth Scientists*. 1996. doi: 10.17226/9077.

[2] T. W. Stacey Curtis, 'MinEx CRC targets Delamerian Orogen', *Energy & Mining*, Sep. 28, 2020. https://www.energymining.sa.gov.au/industry/geological-survey/mesa-journal/previous_news/news-articles-2019/minex_crc_targets_delamerian_orogen (accessed Jun. 19, 2023).

[3] I. Belousov, R. R. Large, S. Meffre, L. V. Danyushevsky, J. Steadman, and T. Beardsmore, 'Pyrite compositions from VHMS and orogenic Au deposits in the Yilgarn Craton, Western Australia: Implications for gold and copper exploration', *Ore Geol. Rev.*, vol. 79, pp. 474–499, Dec. 2016, doi: 10.1016/j.oregeorev.2016.04.020.

[4] M. Keith, D. J. Smith, G. R. T. Jenkin, D. A. Holwell, and M. D. Dye, 'A review of Te and Se systematics in hydrothermal pyrite from precious metal deposits: Insights into ore-forming processes', *Ore Geol. Rev.*, vol. 96, pp. 269–282, May 2018, doi: 10.1016/j.oregeorev.2017.07.023.

[5] K. F. Cassidy, D. I. Groves, and N. J. McNaughton, 'Late-Archean granitoid-hosted lode-gold deposits, Yilgarn Craton, Western Australia: Deposit characteristics, crustal architecture and implications for ore genesis', *Ore Geol. Rev.*, vol. 13, no. 1, pp. 65–102, Apr. 1998, doi: 10.1016/S0169-1368(97)00014-0.

[6] 'Pyrite', *Wikipedia*. May 23, 2023. Accessed: Jun. 19, 2023. [Online]. Available: https://en.wikipedia.org/w/index.php?title=Pyrite&oldid=1156598133

[7] GEOLOGYSCIENCE, 'Pyrite | Properties, Uses, Occurrence & more...', *Geology Science*, Apr. 30, 2018. https://geologyscience.com/minerals/pyrite/ (accessed Jun. 19, 2023).

[8] C. D. Barrie, A. P. Boyle, N. J. Cook, and D. J. Prior, 'Pyrite deformation textures in the massive sulfide ore deposits of the Norwegian Caledonides', *Tectonophysics*, vol. 483, no. 3, pp. 269–286, Mar. 2010, doi: 10.1016/j.tecto.2009.10.024.

[9] S. Wang *et al.*, 'Ore genesis and hydrothermal evolution of the Shaxi porphyry Cu–Au deposit, Anhui province, Eastern China: evidence from isotopes (S–Sr–H–O), pyrite, and fluid inclusions', *Miner. Deposita*, vol. 56, no. 4, pp. 767–788, Apr. 2021, doi: 10.1007/s00126-020-00995-5.

[10] Q. Zuo *et al.*, 'NanoSIMS sulfur isotope studies of pyrite from the Early Paleozoic marine shale: Implications for the sedimentary environment', *Mar. Pet. Geol.*, vol. 124, p. 104802, Feb. 2021, doi: 10.1016/j.marpetgeo.2020.104802.

[11] Z. Lin *et al.*, 'Effects of sulfate reduction processes on the trace element geochemistry of sedimentary pyrite in modern seep environments', *Geochim. Cosmochim. Acta*, vol. 333, pp. 75–94, Sep. 2022, doi: 10.1016/j.gca.2022.06.026.

[12] R. R. Large, V. V. Maslennikov, F. Robert, L. V. Danyushevsky, and Z. Chang, 'Multistage Sedimentary and Metamorphic Origin of Pyrite and Gold in the Giant Sukhoi Log Deposit, Lena Gold Province, Russia', *Econ. Geol.*, vol. 102, no. 7, pp. 1233–1267, Nov. 2007, doi: 10.2113/gsecongeo.102.7.1233.

[13] D. R. Cooke, P. Hollings, J. J. Wilkinson, and R. M. Tosdal, '13.14 - Geochemistry of Porphyry Deposits', in *Treatise on Geochemistry (Second Edition)*, H. D. Holland and K. K. Turekian, Eds., Oxford: Elsevier, 2014, pp. 357–381. doi: 10.1016/B978-0-08-095975-7.01116-5.
[14] W. Sinclair, 'Porphyry deposits', 2007, pp. 223–243.
[15] R. V. Kirkham, 'Intermineral Intrusions and Their Bearing on the Origin of Porphyry Copper and Molybdenum Deposits', *Econ. Geol.*, vol. 66, no. 8, pp. 1244–1249, Dec. 1971, doi: 10.2113/gsecongeo.66.8.1244.
[16] 'Porphyry copper deposit', *Wikipedia*. Mar. 23, 2023. Accessed: Jun. 19, 2023. [Online]. Available: https://en.wikipedia.org/w/index.php?title=Porphyry_copper_deposit&oldid=1146265879
[17] W. J. McMillan, 'PORPHYRY DEPOSITS'. http://earthsci.org/mineral/mindep/phor_dep/por_dep.html (accessed Jun. 19, 2023).
[18] MAT M., 'Volcanogenic Massive Sulfide (VMS) Deposits » Geology Science', *Geology Science*, Feb. 19, 2023. https://geologyscience.com/geology-branches/mining-geology/volcanogenic-massive-sulfide-vms-deposits/ (accessed Jul. 25, 2023).
[19] 'Volcanogenic massive sulfide ore deposit', *Wikipedia*. May 22, 2023. Accessed: Jul. 25, 2023. [Online]. Available: https://en.wikipedia.org/w/index.php?title=Volcanogenic_massive_sulfide_ore_deposit&oldid=1156451134
[20] J. Foden, M. A. Elburg, J. Dougherty-Page, and A. Burtt, 'The Timing and Duration of the Delamerian Orogeny: Correlation with the Ross Orogen and Implications for Gondwana Assembly', *J. Geol.*, vol. 114, no. 2, pp. 189–210, Mar. 2006, doi: 10.1086/499570.
[21] J. Foden *et al.*, 'Cambro-Ordovician magmatism in the Delamerian orogeny: Implications for tectonic development of the southern Gondwanan margin', *Gondwana Res.*, vol. 81, pp. 490–521, May 2020, doi: 10.1016/j.gr.2019.12.006.
[22] T. Flöttmann, P. Haines, J. Jago, P. James, A. Belperio, and J. Gum, 'Formation and reactivation of the Cambrian Kanmantoo Trough, SE Australia: implications for early Palaeozoic tectonics at eastern Gondwana's plate margin', *J. Geol. Soc.*, vol. 155, no. 3, pp. 525–539, May 1998, doi: 10.1144/gsjgs.155.3.0525.
[23] M. Sandiford, 'CHAPTER 8—Neotectonics of southeastern Australia: linking the Quaternary faulting record with seismicity and in situ stress'.
[24] 'Darling–Curnamona–Delamerian | Exploring for the Future | Geoscience Australia'. https://www.eftf.ga.gov.au/darling-curnamona-delamerian (accessed May 29, 2023).
[25] E. & Mining, 'Data and ground release opens the door', *Energy & Mining*, Oct. 02, 2020. https://www.energymining.sa.gov.au/industry/geological-survey/mesa-journal/previous_news/news-articles-2020/data_and_ground_release_opens_the_door (accessed Sep. 03, 2023).
[26] K. S. Ahmed *et al.*, 'Pyrite Dissolution in the Cretaceous Yogou Formation of the Niger (Chad) Basin: Implications for Basin Evolution under a Rift Tectonic Setting', *ACS Omega*, vol. 7, no. 48, pp. 43411–43420, Dec. 2022, doi: 10.1021/acsomega.2c03027.

[27] I. Belousov, L. Danyushevsky, P. Olin, SE Gilbert, and J. Thompson, 'STDGL3 - a new calibration standard for sulphide analysis by LA-ICP-MS', Jan. 2015, Accessed: Aug. 09, 2023. [Online]. Available: https://figshare.utas.edu.au/articles/conference_contribution/STDGL3_-_a_new_calibration_standard_for_sulphide_analysis_by_LA-ICP-MS/23144639/1
[28] K. P. Jochum, M. Willbold, I. Raczek, B. Stoll, and K. Herwig, 'Chemical characterisation of the USGS reference glasses GSA-1G, GSC-1G, GSD-1G, GSE-1G, BCR-2G, BHVO-2G and BIR-1G using EPMA, ID-TIMS, ID-ICP-MS and LA-ICP-MS', *Geostand. Geoanalytical Res.*, vol. 29, no. 3, pp. 285–302, 2005, doi: 10.1111/j.1751-908X.2005.tb00901.x.
[29] D. D. Gregory *et al.*, 'Distinguishing Ore Deposit Type and Barren Sedimentary Pyrite Using Laser Ablation-Inductively Coupled Plasma-Mass Spectrometry Trace Element Data and Statistical Analysis of Large Data Sets', *Econ. Geol.*, vol. 114, no. 4, pp. 771–786, Jun. 2019, doi: 10.5382/econgeo.4654.
[30] N. J. Cook, C. L. Ciobanu, and J. Mao, 'Textural control on gold distribution in As-free pyrite from the Dongping, Huangtuliang and Hougou gold deposits, North China Craton (Hebei Province, China)', *Chem. Geol.*, vol. 264, no. 1, pp. 101–121, Jun. 2009, doi: 10.1016/j.chemgeo.2009.02.020.
[31] M. Ishida *et al.*, 'Auriferous pyrite formed by episodic fluid inputs in the Akeshi and Kasuga high-sulfidation deposits, Southern Kyushu, Japan', *Miner. Deposita*, vol. 57, no. 1, pp. 129–145, Jan. 2022, doi: 10.1007/s00126-021-01053-4.
[32] J. Liu *et al.*, 'Cracking mechanisms during galena mineralization in a sandstone-hosted lead-zinc ore deposit: Case study of the Jinding giant sulfide deposit, Yunnan, SW China', *Miner. Deposita*, vol. 45, pp. 567–582, Aug. 2010, doi: 10.1007/s00126-010-0294-7.
[33] J. Alonso-Azcárate, M. Rodas, L. Fernández-Díaz, S. h. Bottrell, J. R. Mas, and S. López-Andrés, 'Causes of variation in crystal morphology in metamorphogenic pyrite deposits of the Cameros Basin (N Spain)', *Geol. J.*, vol. 36, no. 2, pp. 159–170, 2001, doi: 10.1002/gj.889.
[34] L. Zhou, C. A. McKenna, D. G. F. Long, and B. S. Kamber, 'LA-ICP-MS elemental mapping of pyrite: An application to the Palaeoproterozoic atmosphere', *Precambrian Res.*, vol. 297, pp. 33–55, Aug. 2017, doi: 10.1016/j.precamres.2017.05.008.
[35] W. U. Reimold, 'Exogenic and endogenic breccias: a discussion of major problematics', *Earth-Sci. Rev.*, vol. 43, no. 1, pp. 25–47, Mar. 1998, doi: 10.1016/S0012-8252(97)00037-8.
[36] V. V. Maslennikov *et al.*, 'Mineralogical Features of Ore Diagenites in the Urals Massive Sulfide Deposits, Russia', *Minerals*, vol. 9, no. 3, Art. no. 3, Mar. 2019, doi: 10.3390/min9030150.
[37] Y. Zhu, F. An, and J. Tan, 'Geochemistry of hydrothermal gold deposits: A review', *Geosci. Front.*, vol. 2, no. 3, pp. 367–374, Jul. 2011, doi: 10.1016/j.gsf.2011.05.006.
[38] J. A. Steadman *et al.*, 'Pyrite trace element behavior in magmatic-hydrothermal environments: An LA-ICPMS imaging study', *Ore Geol. Rev.*, vol. 128, p. 103878, Jan. 2021, doi: 10.1016/j.oregeorev.2020.103878.
[39] G. Loftus-Hills and M. Solomon, 'Cobalt, nickel and selenium in sulphides as indicators of ore genesis', *Miner. Deposita*, vol. 2, no. 3, pp. 228–242, Nov. 1967, doi: 10.1007/BF00201918.

[40] 'Hydrothermal alteration and mineralisation characteristics at Anabama Hill: a porphyry Cu-Mo prospect in the Delamerian Orogen, South Australia – 2021 AESC'. https://aesconvention.com.au/hydrothermal-alteration-and-mineralisation-characteristics-at-anabama-hill-a-porphyry-cu-mo-prospect-in-the-delamerian-orogen-south-australia/ (accessed Aug. 28, 2023).
[41] 'Precompetitive-Review-Delamerian-NDI-campaign-hits-its-mark_-Fe-and-Cu-sulphides-extensive-porphyry-Cu-style-alteration-and-a-VMS-pla.pdf'. Accessed: Aug. 28, 2023. [Online]. Available: https://minexcrc.com.au/wp-content/uploads/2022/10/Precompetitive-Review-Delamerian-NDI-campaign-hits-its-mark_-Fe-and-Cu-sulphides-extensive-porphyry-Cu-style-alteration-and-a-VMS-pla.pdf
[42] D. L. Huston, S. H. Sie, G. F. Suter, D. R. Cooke, and R. A. Both, 'Trace elements in sulfide minerals from eastern Australian volcanic-hosted massive sulfide deposits; Part I, Proton microprobe analyses of pyrite, chalcopyrite, and sphalerite, and Part II, Selenium levels in pyrite; comparison with delta 34 S values and implications for the source of sulfur in volcanogenic hydrothermal systems', *Econ. Geol.*, vol. 90, no. 5, pp. 1167–1196, Aug. 1995, doi: 10.2113/gsecongeo.90.5.1167.
[43] B. Cave, R. Lilly, and K. Barovich, 'Textural and geochemical analysis of chalcopyrite, galena and sphalerite across the Mount Isa Cu to Pb-Zn transition: Implications for a zoned Cu-Pb-Zn system', *Ore Geol. Rev.*, vol. 124, p. 103647, Sep. 2020, doi: 10.1016/j.oregeorev.2020.103647.

Appendices

Appendix A: Laser ablated spots on samples collection by LA-ICP-MS
https://liveuclac-my.sharepoint.com/:p:/g/personal/ucecszo_ucl_ac_uk/EfnKhCKG9mtIhj2Gso5v_HkBDFpFj095MseInFaoPE02mA?e=98H69q

Appendix B: LA-ICP-MS Results of Key Elements of pyrite
https://liveuclac-my.sharepoint.com/:x:/g/personal/ucecszo_ucl_ac_uk/ESquTw9EzqpIuQxKpU2SoMIBkmGFSt2ETxE5Kaefn4-QDQ?e=hmDNRs